Comparative analysis reveals Ce3D as optimal clearing method for in toto imaging of the mouse intestine

Comparative analysis reveals Ce3D as optimal clearing method for in toto imaging of the mouse intestine.

Gleison D. P. Bossolani[1,2*], Isabel Pintelon[1*], Jan D. Detrez[1], Roeland Buckinx[1], Sofie Thys[1], Jacqueline Nelisis Zanoni[2], Winnok H. De Vos[1], Jean-Pierre Timmermans[1]

[1]Laboratory of Cell Biology and Histology, Department of Veterinary Sciences, University of Antwerp, Antwerp, Belgium

[2]Department of Morphological Sciences, State University of Maringá, Maringá, Paraná, Brasil

*both authors contributed equally

Author correspondence:

Prof. Dr. Jean-Pierre Timmermans

University of Antwerp, Belgium

Department of Veterinary Sciences

Laboratory of Cell Biology and Histology

Universiteitsplein 1, B-2610 Wilrijk

jean-pierre.timmermans@uantwerpen.be

ABBREVIATIONS

2D: two-dimensional

3D: three-dimensional

BABB: benzyl alcohol/benzyl benzoate

BABB-D15: BABB/diphenyl ether (1:15)

BSA: bovine serum albumin

DBE: dibenzyl ether

DCM: dichloromethane

DMSO: dimethyl sulfoxide

DPE: diphenyl ether

ENS: enteric nervous system

GFP: green fluorescent protein

GI: gastrointestinal

HE: hematoxylin-eosin

NHS: normal horse serum

PBS: phosphate-buffered saline

PBST: PBS containing 0.2% Triton X-100 and 20% DMSO

PFA: paraformaldehyde

PTwH: PBS/0.2% Tween-20 with 10 mg/ml heparin

RI: refractive index

RIMS: refractive index matching solution

RT: room temperature

SEM: scanning electron microscope

THF: tetrahydrofuran

V: volume

Key Points

1. Visikol®, ScaleS- and CUBIC-cleared mouse intestinal samples yield low to modest optical penetration depth, not allowing whole-thickness imaging of the intestinal wall and resulting in substantial structural deformation of the mucosal (sub)epithelial layer.
2. The 3DISCO, iDISCO+ and uDISCO clearing protocols render 1.5-mm-thick samples of the intact mouse intestinal wall fully transparent but equally suffer from destructive tissue effects (e.g. shrinkage and damage to tissue morphology).
3. The hydrophylic clearing protocols Ce3D, SeeDB2 and UbasM result in excellent GFP retention and preservation of morphology as well as antigenicity and fluorescent staining. Only Ce3D renders full-thickness tissue homogeneously transparent.
4. Ce3D emerged as the most efficient, low-toxic and least time-consuming, cheap protocol for full-thickness 3D mapping of the gastrointestinal wall.

ABSTRACT

Background: The intestinal wall has a complex topographical architecture. The multi-layered network of the enteric nervous system and its intercellular interactions are difficult to map using traditional section-based or whole-mount histology. With the advent of optical clearing techniques, it has become feasible to visualize intact tissue and organs in 3D. However, as yet, a gap still needs to be filled in that no in-depth analysis has been performed yet on the potential of different clearing techniques for the small intestine.

Aim: The goal of this study was to identify an optimal clearing protocol for *in toto* imaging of mouse intestinal tissue.

Methods: Five aqueous-based clearing protocols (SeeDB2, CUBIC, ScaleS, Ce3D and UbasM) and four organic reagent-based clearing protocols (3DISCO, iDISCO+, uDISCO and Visikol®) were assessed in segments of small intestine from CX3CR1$^{GFP/GFP}$ and wild-type mice. Following clearing, optical transparency, tissue morphology, green fluorescent protein (GFP) fluorescence retention and compatibility with (immuno-)labeling were analysed.

Key results: All organic reagent-based clearing protocols – except for Visikol – rendered tissue highly transparent but led to substantial tissue shrinkage and deformation. Of the aqueous-based protocols, only Ce3D yielded full-thickness tissue transparency. In addition, Ce3D displayed excellent GFP retention and preservation of tissue morphology.

Conclusions: Ce3D emerged as a most efficient protocol for enabling rapid full-thickness 3D mapping of the mouse intestinal wall.

Key words: optical clearing, tissue transparency clearing capability, tissue morphology, GFP preservation, Ce3D, in toto imaging.

INTRODUCTION

Until recently, the topographical architecture of the enteric nervous system (ENS) and its interactions with other intramural components such as the mucosal barrier, the muscle and immune cells could only be visualized with 2D histological techniques, based on thin cross-sections or whole-mount preparations. However, 2D techniques are invasive, artefact-prone, and complicate the interpretation of complex 3D architectures (**1-7**). In recent years, tissue clearing has re-emerged as a powerful tool for bypassing tissue sectioning. This has led to the development of a plethora of tissue clearing protocols that reduce optical scattering ~~and photon absorption~~ by extracting the lipid fraction and/or by refractive index matching thereby yielding full-thickness tissue transparency (**4, 7-14**). These protocols allow detailed 3D visualization of intact organs by confocal, light-sheet or two-photon microscopy, but the appropriateness of each method is organ-specific and depends on the aspired goal in terms of clearing capability, preservation of fluorescent reporter protein signal, compatibility with immunolabeling and nuclear staining, morphological tissue integrity, complexity and cost (**6, 14**).

Despite the rapid and efficient clearing of large samples, the use of organic solvent-based clearing methods such as BABB (**15**), 3DISCO (**16, 17**), Visikol (**18**) and iDISCO(+) (**19, 20**) is typically associated with tissue shrinkage and quenching of fluorescent proteins (**4**). Moreover, the toxic nature of these organic solvents requires careful sample handling and limits the compatibility with immersion objectives. Although advances were made to overcome these disadvantages (**20, 21**), dehydration methods still suffer from sample shrinkage and ultrastructural damage remains unaddressed. To overcome these limitations, a novel category of clearing approaches based on aqueous solutions has been developed: SeeDB/SeeDB2 (**22, 23**), ClearT/ClearT2 (**24**), CUBIC and derived protocols (**25, 26**) including UbasM (**11**), Scale/ScaleS (**27, 28**) and Ce3D

(**14**). Whereas the earlier protocols (SeeDB, ClearT2 and Scale) were still hampered by modest clearing capability and GFP preservation (**7, 29**), CUBIC and its modifications yielded better clearance (**26**). The more recently developed protocols (SeeDB2, ScaleS, Ce3D and UbasM) have been reported to show superior outcomes in terms of clearing capability, GFP retention and morphological preservation (**11, 14, 23, 28**). CLARITY and derived protocols compose a third category of clearing approaches, which involves the embedding of intact tissue into a hydrogel (**30-33**). Although these protocols aim to further improve tissue transparency with minimal protein loss, they are more time-demanding or require additional infrastructure (**7, 29**).

As far as the GI tract is concerned, a systematic benchmark of different clearing methods is lacking. Clearing of gut tissue has been performed with variable results and for specific aims using different approaches or modifications of existing protocols including FocusClear (**1-3, 34-38**), BABB-based methods (**39**), urea-based ScaleA2 and SeeDB (**38**), the PACT variant of CLARITY (**32**) and RIMS (**40**). Therefore, the aim of this study was to evaluate and directly compare the performance of the most effective, state-of-the-art clearing protocols) on intestinal tissue. The outcome of this study provides a methodological guideline for researchers interested in exploring and visualizing connections and interactions in the intestinal wall through 3D image reconstruction and analysis.

MATERIALS AND METHODS

Tissue collection

All animal handling and housing procedures were conducted in accordance with European directive 86/609/EEC. The small intestine was obtained from adult CX3CR1$^{GFP/GFP}$ (**41**) and wild-type C57BL/6 mice. Animals were housed in controlled environmental conditions of temperature (22 °C) and illumination (12/12h light-dark cycle). All mice received food and water *ad libitum*. Animals were sacrificed by cervical dislocation and the ileum was collected and washed in ice-cold Krebs solution (117 mM NaCl, 5 mM KCl, 2.5 mM $CaCl_2 \cdot 2H_2O$, 1.2 mM $MgSO_4 \cdot 7H_2O$, 25 mM $NaHCO_3$, 1.2 mM $NaH_2PO_4 \cdot 2H_2O$, and 10 mM glucose; pH 7.4). Afterwards, intestinal samples were opened along the mesenteric border and fixed with pins in a Sylgard-coated Petri dish. Subsequently, tissues were fixed in 4% paraformaldehyde (PFA) for 2h at 4 °C, washed with 0.01M phosphate-buffered saline (PBS; pH 7.4), and cut into segments of 1 cm length for tissue clearing.

Immunostaining and nuclear staining of intestinal whole-mounts

In general, the immunolabelling procedure preceded the clearing protocols, except for CUBIC, UbasM and Ce3D (see below). Nuclear counterstaining with TO-PRO-3 or DAPI was used for assessment of optical penetration depth across the intestinal layers. For immunofluorescent staining, a single neuronal immunostaining (ßIII-tubulin-Cy3-immunostaining) or double staining with either an endothelial marker (CD31) or a fibroblast-like cell marker (PDGFR-α) was performed for all clearing protocols to test its compatibility with immunostaining. Additionally, the compatibility with the different clearing protocols of frequently used neurochemical markers used for subtyping cells in the intestinal wall were tested as well. In general, after an overnight blocking step,

intestinal samples were incubated in primary antibody dilutions for 2 days, rinsed in between and then followed by an overnight incubation in the secondary antibody solutions. The exact protocols of immunostaining procedures were slightly adapted to the clearing protocol used and are described in more detail in the respective paragraphs. The primary and secondary antibodies used in this study are listed in Table 1.

Tissue permeabilization

Tissue permeabilization for 3DISCO, iDISCO+, uDISCO and Visikol protocols was performed including either sample pretreatment with methanol or an alternative pretreatment protocol without methanol according to Renier and colleagues (**19**). In the first method, intestinal samples were rinsed 3x30 min in 0.01M PBS (pH 7.4), followed by permeabilization in a graded series of 20%, 40%, 60%, 80% and 2x 100% methanol on a shaker at RT (1h for each step). The samples were then rehydrated in a reversed methanol series (80%, 60%, 40%, 20%) and further permeabilized in PBS containing 0.2% Triton X-100 and 20% DMSO (PBST) for 2x1 h. In the methanol-free method, intestinal tissues were rinsed 3x30 min in PBS and then 2x1 h in PBST, followed by overnight incubation in PBST at 37 °C. Subsequently, the tissues were incubated in PBS containing 0.1% Tween-20, 0.1% Triton X-100, 0.1% deoxycholate, 0.1% NP40 and 20% DMSO, at 37 °C overnight, and then rinsed 2x1 h in PBS, containing 0.2% Triton X-100 for 1 h before the onset of further immunostaining procedures.

Immunostaining and nuclear staining

The immunostaining protocol for 3DISCO, iDISCO+, uDISCO was performed according to Renier and colleagues (**19**). To block any residual active aldehyde groups, intestinal samples were incubated overnight in PBS/0.2% Triton X-100/20% DMSO/0.3

M glycine at 37 °C and then blocked for 1 day in PBS/0.2% Triton X-100/10% DMSO/6% Normal Horse Serum (NHS) at 37 °C. After blocking, intestinal samples were rinsed twice in PBS/0.2% Tween-20 with 10 mg/ml heparin (PTwH) for 1 h, followed by incubation for 2 days in primary antibody solution (PTwH, containing 5% DMSO and 3% NHS), at 37 °C. Ileal segments were then rinsed 5x30 min in PTwH and incubated overnight in secondary antibody dilutions in PTwH containing 3% NHS at 37 °C. Samples were finally washed 5x30 min in PTwH prior to counterstaining with TO-PRO-3 (1:500 in PTwH) for at least 5 h. Finally, tissues were washed 5x30 min in PTwH. After the staining procedure, clearing was performed as detailed below.

Tissue clearing

The 3DISCO clearing protocol was carried out at RT under continuous gentle shaking (**16**). For iDISCO+ and uDISCO clearing we used the protocols described by Renier and colleagues (**19**) and Pan and colleagues (**21**), respectively. The Visikol clearing procedure was performed according to manufacturer's instructions (Visikol, Whitehouse Station, NJ, USA).

For ScaleS and SeeDB2 clearing the protocols of Hama and colleagues (**28**) and Ke and colleagues (**22**) were applied, respectively. The CUBIC and UbasM clearing procedures were carried out according to the protocols described by Susaki and colleagues (**26**) and Chen and colleagues (**11**), respectively.

The Ce3D procedure involved incubation of intestinal samples for 8 h in a blocking solution containing 0.01M PBS/1% NHS/1% BSA/0.3% Triton X-100. For immunostaining, tissues were incubated in the primary antibody solution (0.01M PBS/1% NHS/ 1% BSA/0.3% Triton X-100/primary antibody) and then washed in 0.01M PBS/0.2% Triton-X100/0.5% 1-thioglycerol (Ce3D washing solution) for 3x10 min.

Subsequently, the intestinal tissues were incubated in the secondary antibody solution, which contained 0.01M PBS/0.3% Triton X-100/secondary antibody. The samples were then again rinsed in Ce3D washing solution for 3x10 min and then counterstained with either DAPI or TO-PRO-3 (1:500) for at least 1 h. Subsequently, ileal segments were again washed in Ce3D washing solution for 5x30 min. Stained tissues were immersed in the Ce3D medium for 12 h at RT and imaged in Ce3D medium (**14**). Note that the N-methylacetamide that is used in the Ce3D solution has high reproductive toxicity and that the N-methylacetamide produces toxic nitrogen oxide fumes when heated.

Macroscopic evaluation of transparency and tissue shrinkage

For macroscopic estimation of the degree of tissue transparency/opaqueness and tissue shrinkage/swelling 4% PFA-fixed ileal tissues, approximately 1 cm in length, were photographed in a transparent Petri dish above a standard grid allowing comparison of the transparency and tissue morphology achieved before and after the clearing procedures. Pictures were analyzed using Image-Pro Plus version 4.5.0.29 (Media Cybernetics, Silver Spring, MD, USA). Data were expressed as mean ± standard deviation (SD).

Confocal microscopy and data acquisition

Fixed intestinal samples, opened along the mesenteric attachment were visualized with a Leica SP8/LMS confocal microscope (Leica Microsystems CMS GmbH, Germany). Samples were positioned in a glass bottom Petri dish, submerged in their respective RI matching solution and covered by a golden ring with nylon mesh to prevent the tissue from floating. To evaluate the optical penetration depth, 300 image stacks (z

step size ~ 1.5 μm) of TO-PRO-3 counterstained samples with a 512x512 pixel resolution (X and Y pixel size is 1.12 μm) at an excitation wavelength of 640 nm were recorded using a 20x/0.75 HC PL Apo objective lens with a working distance of 600 μm. Immersion oil and glycerol solution (80%) were used for the four organic reagent-based clearing protocols and the five aqueous-based clearing protocols, respectively. The correction collar of this multi-immersion objective was adjusted accordingly to match the refractive index of oil (RI~1.52) or 80% glycerol (RI~1.46). Thirty high-resolution image stacks (z step size ~ 1 μm) with 1024x1024 pixel resolution were collected for imaging of the specific layers of the intestinal whole-mounts.

GFP fluorescence quantification

After immunostaining and clearing, the retention of GFP fluorescence intensity in CX3CR1-positive mononuclear phagocytes of intestinal whole-mounts of CX3CR1-GFP transgenic mice was measured using ImageJ image processing freeware (National Institutes of Health, Bethesda, MD, USA). In brief, Z-stacks of microvilli were projected along the axial axis according to the maximum pixel intensity. Subsequently, a fixed intensity threshold was set, just above background fluorescence, and the average intensity of the objects detected above this threshold was measured. The average object intensity was expressed relative to the background threshold value (i.e. GFP intensity ratio). Non-cleared samples were used as controls to evaluate the GFP preservation of each clearing protocol. Statistical analyses were performed using GraphPad Prism 6 software. All data were expressed as mean ± standard error (SEM). A non-parametric t-test was used and values with $p < 0.05$ were considered statistically significant.

Morphological damage assessment by hematoxylin-eosin (HE) staining and scanning electron microscopy (SEM)

To assess morphological damage at the light microscopical level, organic solvent-based cleared tissues were washed in 100% ethanol for 3x10 min and were then further processed for paraffin embedding, sectioned (5 µm) and stained for HE. Hydrophilic reagent-based cleared tissues had to be dehydrated first in a graded alcohol series before paraffin-embedding, subsequent sectioning and HE staining. For SEM, cleared samples, previously fixed in 4% PFA, were washed 3x30 min in 0.01M PBS and additionally fixed for 72 h at 4°C in 2.5% glutaraldehyde in 0.1 M Na-cacodylate buffer, dehydrated, critical point dried, gold-sputtered and viewed in a Quanta FEG250 SEM system (ThermoFisher Scientific).

RESULTS

Morphological preservation

Macroscopic images from intestinal samples before and after clearing taken on a mm-grid show that the mm-grid is less visible in the images of Visikol and ScaleS. All other protocols resulted in full transparency of the tissue. The highest shrinkage rates were observed for the organic solvent-based DISCO clearing procedures (3DISCO 57.16 ± 9.8%; iDISCO+ 32.25 ± 20.5%; µDISCO 43.60 ± 10.5% and Visikol 18.18 ± 9.8%), whereas much less shrinkage was observed after ScaleS and Ce3D clearing (6.65 ± 7.3, 5.40 ± 6.0% respectively) (Fig. 1). UbasM-, SeeDB2- and CUBIC-based clearing procedures resulted in a substantial (UbasM) or slight (SeeDB2 and Cubic) increase of tissue area (41.09 ± 7.1%, 4.32 ± 3.8% and 4.35 ± 2.6% respectively) (Fig. 1). In addition, in contrast to the 3DISCO and Ce3D procedures, CUBIC, iDISCO+ (not shown) and uDISCO produced significant destructive effects on the mucosal villi as observed on the SEM and HE images (Fig. 3). Tissue structural deformations induced by dehydration and delipidation procedures were also seen upon macroscopic examination, mainly for the 3DISCO- and uDISCO-cleared samples (Fig. 1).

Clearing capacity and optical penetration depth

Optical penetration depth analysis showed that only 3DISCO, iDISCO, uDISCO and Ce3D achieved full-thickness optical transparency of the intestinal whole-mounts (Fig. 2). The clearing capacity of the UbasM procedure yielded comparable results to the procedures mentioned above in specific areas but appeared not homogeneous for all different layers in the intestinal whole-mounts resulting in inhomogeneous fluorescent staining (Fig. 2 and Suppl Fig.).

GFP fluorescence preservation/quantification

297 For organic solvent-based clearing protocols, two distinct pretreatments of
298 intestinal tissues have been reported for tissue permeabilization, based on either a
299 dehydration/rehydration procedure with methanol or alternative pretreatment using an
300 aqueous solution that contained PBS, detergent series and DMSO (**19**). The earlier
301 reported significant GFP quenching effect of methanol (**4, 42, 43**) was also confirmed in
302 our study. Consequently, we selected the alternative pretreatment without methanol for
303 comparative GFP quantification. Estimates of GFP fluorescence, based on comparison of
304 maximum intensity projection images of the different procedures, showed that Ce3D and
305 SeeDB2 led to significantly lower GFP quenching compared to 3DISCO, uDISCO,
306 iDISCO+, Visikol, CUBIC and ScaleS (Fig. 4).

307 **Compatibility of the clearing protocols with immunostaining**

308 Double immunostainings with the neuronal marker ßIII-tubulin and either the
309 endothelial marker CD31 or the fibroblast-like cell marker PDGFR-α were performed in
310 combination with the nuclear stain DAPI on intestinal whole-mounts of CX3CR1-GFP
311 transgenic mice (Fig. 5). Ce3D clearing allowed the simultaneous visualization of both
312 the submucosal and myenteric enteric nerve network at the distinct topographical levels
313 and its close interactions and associations with epithelial, immune and vascular
314 components (Fig 5; Suppl video). In addition to the above-mentioned markers, other
315 frequently used neurochemical markers (S100, GFAP, nNOS, NF200, Vimentin, c-kit,
316 calretinin and calbindin) were tested as well (see Table 1; data not shown) and all these
317 antibodies showed compatibility with the Ce3D clearing protocol.

318 **Comparison of the clearing protocols in terms of duration, handling and safety**

319 Additional comparison of the remaining protocols in terms of clearing time,
320 technical handling and safety requirements revealed that SeeDB2 and Ce3D were the
321 preferable methods (see Table 2, Suppl Fig.). In contrast to organic solvent-based clearing

protocols, these water-based clearing procedures involve the use of reagents that are non-irritant and less ~~non-~~toxic and require less immersion steps, although it should be noted that one component in the Ce3D solution, i.e. N-methylacetamide, does have toxic features and might produce toxic nitrogen oxide fumes when heated (which is required in the protocol). Compared to the other protocols requiring a minimum incubation time ranging from a few days to 1 week, Ce3D required the shortest clearing time (12h) with good morphological preservation and compatibility with GFP and different antibodies tested~~.~~

DISCUSSION

The applicability of 9 clearing techniques (4 organic solvent-based and 5 aqueous-based protocols) was evaluated for 3D visualization of the entire thickness of the intestinal wall in terms of the following parameters: tissue clearing efficiency, preservation of tissue morphology and GFP fluorescence, immuno- and nuclear staining compatibility, clearing protocol time and safety of the chemical reagents used. CLARITY-based protocols have not been performed in this study, since these are protocols that are more time-consuming or require additional dedicated (commercially available) equipment and have been reported to lead to GFP quenching, ultrastructural changes and compromised structural integrity due to aggressive lipid removal from the biological samples (**7, 23, 29**).

In line with data reported in other organs (**6, 14, 16, 17, 19, 21, 29, 44**), of all 9 optical clearing techniques compared in this study, 3DISCO, iDISCO+, uDISCO and Ce3D showed the highest and most homogeneous clearing capacity. In terms of visualization of full-thickness intestinal samples, the Ce3D protocol equally yielded better clearing results compared to SeeDB2 (**23**). Compared to the original CUBIC protocol, its improved version UbasM did result in higher transparency of the intestinal tissue and less morphological damage (similar to the Ce3D protocol), but suffered from inhomogeneous clearing throughout the intestinal wall. The inferior results in clearing capacity for ScaleS and in particular for Visikol, observed in our experiments on mouse intestine, indicate that its clearing performance is tissue-specific, since better results with these protocols were obtained in brain tissue (**28, 45**). This tissue dependence might be explained by differences in lipid content, pigment, or the degree of inhomogeneity in refractive index (**4**).

Despite having excellent clearing capacity and providing good results in the brain, the distinct DISCO protocols are less suitable to obtain optimal images of the full-thickness intestinal wall due to the destructive effects they have on intestinal samples (e.g. damage in mucosal epithelium ~~and/or membrane integrity,~~ and substantial tissue shrinkage). It has been reported that the potent clearing properties of 3DISCO, iDISCO+ and uDISCO, which might be an advantage for brain tissue, may lead to destructive effects on biological (sub)cellular structures, due to the aggressive properties of a.o. methanol, THF and DCM (**10, 11, 45**). Similarly, in line with earlier reports on other tissues (**8, 11, 28, 35, 46**) the CUBIC protocol affected the morphology of the intestinal samples, limiting compatibility of these protocols for post-hoc correlative ultrastructural studies.

Substantial or even complete loss of GFP fluorescence occurred in intestinal samples of CX3CR1 transgenic mice after 3DISCO, iDISCO+, uDISCO and Visikol clearing, which is in line with previous findings in other tissues (**11, 13, 14, 28, 29, 46, 47**). Therefore, taken together with their destructive effects on morphology, these protocols were not further considered for testing their compatibility with immunostaining with intestinal neurochemical markers. Of the 5 aqueous-based protocols, urea-based methods such as ScaleS and CUBIC equally induced substantial GFP quenching, probably due to the presence of the high detergent concentration and the denaturating properties of urea (**7, 29, 46, 48**). In this study, only UbasM (using much lower detergent concentrations compared to CUBIC), SeeDB2 and Ce3D (both using iohexol solutions) met the requirements in terms of GFP signal retainment, as was also found for other fluorescent reporters (**23, 49**). The latter three protocols were also compatible with immunostaining procedures enabling the visualization of the intrinsic enteric network and its interaction with blood vessels, immune cells and the distinct components of the

mucosal barrier. The aqueous-based clearing procedures were also superior to the ~~non-aqueous~~ organic solvent-based protocols in terms of long-term storage due to the more aggressive solvents which have a strong negative impact on antigenicity (**29**).

In conclusion, Ce3D emerged as the preferred clearing protocol for 3D imaging of full-thickness intestinal segments, since it is a non-destructive, cost-effective and fast clearing technique with excellent GFP signal preservation and immuno- and nuclear counterstaining compatibility. Thus, it provides a promising tool for studying the distinct intramural components in the GI tract in healthy and diseased conditions. This 3D imaging approach of full-thickness samples opens avenues for detailed mapping and distributional analysis of distinct subsets of cells of the neuro-immune-vascular interactive network within the entire GI wall, thereby leading to a better understanding of the pathophysiological changes occurring in specific GI disorders.

ACKNOWLEDGMENTS

The authors thank Danny Vindevogel and Dominique De Rijck for administrative and technical support. The authors would also like to thank the Electron Microscopy for Material Science group (Prof Dr Sara Bals) at the University of Antwerp for the use of the environmental SEM (Quanta 250 FEG). The Quanta 250 FEG (Hercules grant AUHA.11.01) and the Leica SP 8 (Hercules grant AUHA.15.12) microscopes were funded by the Hercules Foundation of the Flemish Government.

FUNDING

This study was supported by grants from CAPES (Coordenação de Aperfeiçoamento de Pessoal de Nível Superior) and Research funding of the University of Antwerp (TTBOF/29267) and VLAIO Baekeland (IWT140775).

COMPETING INTERESTS

The authors declare no competing interests.

AUTHOR CONTRIBUTION

GB, IP and ST performed experiments and participated in data analysis. RB and JPT designed the study. GB, RB and JPT wrote the largest part of the manuscript. JD, IP, JZ, RB, WDV and JPT critically revised the manuscript. RB, WDV and JPT provided essential research tools, research infrastructure and funding for this study.

REFERENCES

1. Fu YY, Tang SC. Optical clearing facilitates integrated 3D visualization of mouse ileal microstructure and vascular network with high definition. *Microvasc Res*. 2010;**80**:512-21.
2. Fu YY, Peng SJ, Lin HY, Pasricha PJ, Tang SC. 3D imaging and illustration of mouse intestinal neurovascular complex. *Am J Physiol Gastrointest Liver Physiol*. 2013;**304**:G1-11.
3. Liu YA, Chen Y, Chiang AS, Peng SJ, Pasricha PJ, Tang SC. Optical clearing improves the imaging depth and signal-to-noise ratio for digital analysis and three-dimensional projection of the human enteric nervous system. *Neurogastroenterol Motil*. 2011;**23**:e446-57.
4. Richardson DS, Lichtman JW. Clarifying tissue clearing. *Cell*. 2015;**162**:246-57.
5. Richardson DS, Lichtman JW. Snapshot: tissue clearing. *Cell* 2017;**171**:496-496.e.1
6. Ariel P. A beginner's guide to tissue clearing. *Int J Biochem Cell Biol*. 2017;**84:**35-9.
7. Tainaka K, Kuno A, Kubota SI, Murakami T, Ueda HR. Chemical principles in tissue clearing and staining protocols for whole-body cell profiling. *Annu Rev Cell Dev Biol*. 2016;**32**:713-41.
8. Orlich M, Kiefer F. A qualitative comparison of ten tissue clearing techniques. *Histol Histopathol*. 2018;**33**:181-99.
9. Aoyagi Y, Kawakami R, Osanai H, Hibi T, Nemoto T. A rapid optical clearing protocol using 2,2'-thiodiethanol for microscopic observation of fixed mouse brain. *PLoS One*. 2015;**10**:e0116280.

445 10. Azaripour A, Lagerweij T, Scharfbillig C, Jadczak AE, Willershausen B, Van
446 Noorden CJ. A survey of clearing techniques for 3D
447 imaging of tissues with special reference to connective tissue. *Prog Histochem*
448 *Cytochem*. 2016;**51**:9-23.
449 11. Chen L, Li G, Li Y, Li Y, Zhu H, Tang L, French P, McGinty J, Ruan S.
450 UbasM: An effective balanced optical clearing method for intact biomedical
451 imaging. *Sci Rep*. 2017;**7**:12218.
452 12. Feuchtinger A, Walch A, Dobosz M. Deep tissue imaging: a review from a
453 preclinical cancer research perspective. *Histochem Cell Biol*. 2016;**146**:781-806.
454 13. Kakimoto T. Validation of an easily applicable three-dimensional
455 immunohistochemical imaging method for a mouse brain using conventional
456 confocal microscopy. *Histochem Cell Biol*. 2018;**149**:97-103.
457 14. Li W, Germain RN, Gerner MY.
458 Multiplex, quantitative cellular analysis in large tissue volumes with clearing-
459 enhanced 3D microscopy (Ce3D). *Proc Natl Acad Sci*. 2017;**114**:E7321-30.
460 15. Becker K, Jährling N, Saghafi S, Weiler R, Dodt H-U. Chemical clearing and
461 dehydration of GFP expressing mouse brains. *PLoS One* 2012;**7**: e33916.
462 16. Ertürk A, Becker K, Jährling N, Mauch CP, Hojer CD, Egen JG, Hellal
463 F, Bradke F, Sheng M, Dodt HU. Three-dimensional imaging of solvent-
464 cleared organs using 3DISCO. *Nat Protoc*. 2012;**7**:1983-95.
465 17. Ertürk A, Bradke F. High-resolution imaging of entire organs by 3-
466 dimensional imaging of solvent cleared organs (3DISCO). *Exp*
467 *Neurol*. 2013;**242**:57-64.

468 18. Villani TS, Koroch AR, Simon JE. An improved clearing and mounting solution
469 to replace chloral hydrate in microscopic applications. *Appl Plant*
470 *Sci*. 2013;**1**:1300016.
471 19. Renier N, Wu Z, Simon DJ, Yang J, Ariel P, Tessier-Lavigne M. iDISCO: a
472 simple, rapid method to immunolabel large tissue samples for volume imaging.
473 *Cell*. 2014;**159**:896-910.
474 20. Renier N, Adams EL, Kirst C, Wu Z, Azevedo R, Kohl J, et al. Mapping of
475 Brain activity by automated volume analysis of immediate early genes. *Cell*
476 2016;**165**:1789–1802.
477 21. Pan C, Cai R, Quacquarelli FP, Ghasemigharagoz A, Lourbopoulos A, Matryba
478 P, Plesnila N, Dichgans M, Hellal F, Ertürk A. Shrinkage-
479 mediated imaging of entire organs and organisms using uDISCO. *Nat*
480 *Methods*. 2016;**13**:859-67.
481 22. Ke MT, Fujimoto S, Imai T. SeeDB: a simple and morphology-
482 preserving optical clearing agent for neuronal circuitre construction. *Nat*
483 *Neurosci*. 2013;**16**:1154-61.
484 23. Ke MT, Nakai Y, Fujimoto S, Takayama R, Yoshida S, Kitajima TS, Sato
485 M, Imai T. Super-resolution mapping of neuronal circuitry with an index-
486 optimized clearing agent. *Cell Rep*. 2016;**14**:2718-32.
487 24. Kuwajima T, Sitko AA, Bhansali P, Jurgens C, Guido W, Mason C. ClearT: a
488 detergent- and solvent-free clearing method for neuronal and non-neuronal
489 tissue. *Development* 2013;**140**:1364-8.
490 25. Susaki EA, Tainaka K, Perrin D, Kishino F, Tawara T, Watanabe
491 TM, Yokoyama C, Onoe H, Eguchi M, Yamaguchi S, Abe T, Kiyonari
492 H, Shimizu Y, Miyawaki A, Yokota H, Ueda HR. Whole-

493 brain imaging with single
494 cell resolution using chemical cocktails and computational analysis.
495 *Cell*. 2014;**157**:726-39.
496 26. Susaki EA, Tainaka K, Perrin D, Yukinaga H, Kuno A, Ueda HR.
497 Advanced CUBIC protocols for whole-brain and whole-
498 body clearing and imaging. *Nat Protoc*. 2015;**10**:1709-27.
499 27. Hama H, Kurokawa H, Kawano H, Ando R, Shimogori T, Noda H, Fukami K,
500 Sakaue-Sawano A, Miyawaki A. Scale: a chemical approach for fluorescence
501 imaging and reconstruction of transparent mouse brain. *Nat Neurosci.*
502 2011;**14**:1481-8.
503 28. Hama H, Hioki H, Namiki K, Hoshida T, Kurokawa H, Ishidate F, Kaneko T,
504 Akagi T, Saito T, Saido T, Myakawi A. Scale S: an optical clearing palette for
505 biological imaging. *Nat*. *Neurosci*. 2015;**18**:1518-29.
506 29. Seo J, Choe M, Kim SY . Clearing and labeling techniques for large-
507 scale biological tissues. *Mol Cells*. 2016;**39**:439-46.
508 30. Chung K, Wallace J, Kim SY, Kalyanasundaram S, Andalman AS, Davidson
509 TJ, Mirzabekov JJ, Zalocusky KA, Mattis J, Denisin AK, Pak S, Bernstein
510 H, Ramakrishnan C, Grosenick L, Gradinaru V, Deisseroth K.
511 Structural and molecular interrogation of intact biological systems.
512 *Nature* 2013;**497**:332-7.
513 31. Tomer R, Ye L, Hsueh B, Deisseroth K.
514 Advanced CLARITY for rapid and high-resolution imaging of intact tissues. *Nat*
515 *Protoc*. 2014;**9**:1682-97.

516 32. Neckel PH, Mattheus U, Hirt B, Just L, Mack AF. Large-
517 scale tissue clearing (PACT): Technical evaluation and new perspectives in imm
518 unofluorescence, histology, and ultrastructure. *Sci Rep*. 2016;**6**:34331.
519 33. Yang B, Treweek JB, Kulkarni RP, Deverman BE, Chen CK, Lubeck E, Shah
520 S, Cai L Gradinaru V. Single-cell phenotyping within transparent intact tissue
521 through whole-body clearing. *Cell*. 2014;**158**:945–958.
522 34. Fu YY, Lin CW, Enikolopov G, Sibley E, Chiang AS, Tang SC. Microtome-
523 free 3-dimensional confocal imaging method for visualization of mouse intestine
524 with subcellular-level resolution. *Gastroenterology* 2009;**137**:453-65.
525 35. Chen Y, Tsai YH, Liu YA, Lee SH, Tseng SH, Tang SC. Application of three-
526 dimensional imaging to the intestinal crypt organoids and biopsied intestinal
527 tissues. *Scientific World Journal*. 2013;**2013**:624342.
528 36. Liu YA, Chung YC, Pan ST, Hou YC, Peng SJ, Pasricha PJ, Tang SC. 3-D
529 illustration of network orientations of interstitial cells of Cajal subgroups in
530 human colon as revealed by deep-tissue imaging with optical clearing. *Am J*
531 *Physiol Gastrointest Liver Physiol*. 2012;**302**:G1099-110.
532 37. Liu YA, Chung YC, Pan ST, Shen MY, Hou YC, Peng SJ, Pasricha PJ, Tang
533 SC3-D imaging, illustration, and quantitation of enteric glial network in
534 transparent human colon mucosa.. *Neurogastroenterol Motil*. 2013;**25**:e324-38.
535 38. Liu CY, Dubé PE, Girish N, Reddy AT, Polk DB.
536 Optical reconstruction of murine colorectal mucosa at cellular resolution. *Am J*
537 *Physiol Gastrointest Liver Physiol*. 2015;**308**:G721-35.
538 39. Appleton PL, Quyn AJ, Swift S, Näthke I. Preparation of wholemount mouse
539 intestine for high-resolution three-dimensional imaging using two-photon
540 microscopy. *J Microsc*. 2009;**234**:196-204.

40. Kaufman JA, Castro MJ, Sandoval-Skeet N, Al-Nakkash L.Optical clearing of small intestine for three-dimensional visualization of cellular proliferation within crypts. *J Anat*. 2018;**232**:152-57.

41. Jung S, Aliberti J, Graemmel P, Sunshine MJ, Kreutzberg GW, Sher A, Littman DR. Analysis of fractalkine receptor CX3CR1 function by targeted deletion and green fluorescent protein reporter gene insertion. *Mol Cell Biol*. 2000;**20**:4106-14.

42. Schwarz M K, Scherbarth A, Sprengel R, Engelhardt J, Theer P, Giesel G. Fluorescent-protein stabilization and high-resolution imaging of cleared, intact mouse brains. *PLoS One* 2015;**10**:e0124650.

43. Lee E, Kim HJ, Sun W. See-Through technology for biological tissue: 3-dimensional visualization of macromolecules. *Int Neurourol J*. 2016;**20**(Suppl 1):S15-22.

44. Ertürk A, Lafkas D, Chalouni C. Imaging cleared intact biological systems at a cellular level by 3DISCO. *J Vis Exp*. 2014;**89**:51382.

45. Johnson M, Villani T. Reversible and non-destructive clearing of rat and mouse brains using Visikol® HISTO™ approach. Rutgers Brain Health Institute Symposium, Rutgers University, 2016, doi.10.13140/RG.2.2.31814.88643.

46. Frétaud M, Rivière L, Job É, Gay S, Lareyre JJ, Joly JS, Affaticati P, Thermes V. High-resolution 3D imaging of whole organ after clearing: taking a new look at the zebrafish testis. *Sci Rep*. 2017;**7**:43012.

47. Kolesová H, Čapek M, Radochová B, Janáček J, Sedmera D. Comparison of different tissue clearing methods and 3D imaging techniques for visualization of GFP-expressing mouse embryos and embryonic hearts. *Histochem Cell Biol*. 2016;**146**:141-52.

48. Yu T, Zhu J, Li Y, Ma Y, Wang J, Cheng X, Jin S, Sun Q, Li X, Gong H, Luo Q, Xu F, Zhao S, Zhu D. RTF:
a rapid and versatile tissue optical clearing method. *Sci Rep*. 2018;**8**:1964.
49. Marx V. Microscopy: seeing through tissue. *Nat Methods* 2014;**11**:1209-14.

LEGENDS

Figure 1. Macroscopic images from intestinal samples before and after clearing, taken on a mm-grid and showing the degree of opaqueness and shrinkage/swelling. The mm-grid is less visible in the images of Visikol and ScaleS compared to the other protocols which all led to full transparent tissue. The three DISCO protocols and Visikol showed large shrinkage of the tissue while UbasM resulted in a substantial swelling. The graph represents the average projected area change (%) for all studied protocols. Mean data ± SD are plotted. iDISCO+, uDISCO, ScaleS (n = 5); 3DISCO, Visikol, SeeDB, CUBIC and UbasM (n = 4) and Ce3D (n = 3).

Figure 2. TOPRO3 staining of full-thickness intestinal samples represented as yz images illustrating the level of transparency. Images were taken with an inverted microscope and the serosa was positioned towards the bottom of the petri-dish. The white dots indicate the borders formed by the serosal layer (z = 0) and the top of the villi (z = 1). Full-depth imaging was achieved with the DISCO protocols and Ce3D. ~~This is also evident from the corresponding graphs that present the changes in intensity of the fluorescence (normalized) over the length of the imaged tissue (z normalized for all graphs). The z~~

~~value that corresponded with the maximal intensity of fluorescence was set as zero; only z values above this point are shown in the graph. The curve of ScaleS is used as a reference (*red line*).~~ Scale bar = 50 µm

Figure 3. Representative images of HE-stained sections and SEM images of non-cleared control and cleared ileal segments. (A), (C), (E), (G), and (I) display HE-stained sections from non-cleared control, 3DISCO, uDISCO, CUBIC and Ce3D, respectively. (B), (D), (F), (H) and (J) show SEM images corresponding to the HE sections. The images of HE-stained sections and SEM unambiguously illustrate the damage to the ~~villus membrane integrity or~~ epithelial mucosa of the villi after clearing with uDISCO and CUBIC (E, F, G, H). On the other hand, the tissue is less affected by 3DISCO and Ce3D procedures as seen in (C), (D), (I) and (J). Inserts depict a more detailed image of the area delineated with the dashed line, corresponding with the top of the villi. Scale bars of the overview images = 100 µm; scale bars of the inserts = 50 µm

Figure 4. Graph representing the degree of GFP preservation of each clearing protocol. To calculate the GFP intensity ratio the average object intensity was expressed relative to the background threshold value. Non-cleared samples were used as controls. This estimate of GFP fluorescence confirmed that the GFP signal was less affected by Ce3D and SeeDB2 protocols. Imaging was performed immediately after finishing the clearing procedure. Mean data ± SEM are plotted. Control (n = 9); iDISCO+, uDISCO, Visikol, SeeDB2, CUBIC, ScaleS and Ce3D (n = 10); 3DISCO, UBASM (n = 5).

Figure 5. ~~Full depth~~ 3D observation showing the epithelium, the enteric nerve network (βIII-tubulin) and its close association with intestinal mononuclear phagocytes (CX3CR1), fibroblast-like cells (PDGFRα) and the vascular network (CD31) in Ce3D-cleared intestinal segments. (A) Full-depth 3D distribution of the intestinal villi and epithelium visualized by DAPI nuclear staining (at the left side of the dotted line). At the right side of the dotted line, the DAPI channel is removed allowing the visualization of the underlying structures, i.e. the underlying neuronal and vascular network as well as $CX3CR1^{+}$ cells across the distinct intestinal layers. A more detailed view of these underlying structures is shown in (B). (C) Bottom view of the myenteric plexus with the deeper located CX3CR1-GFP cells and blood vessels. (D) Similar image as (B) but now showing the fibroblast-like cell network instead of blood vessels. (E) Optical cross-section of an intestinal villus illustrating the intimate network of enteric nerves, ~~blood vessels,~~ immune cells and fibroblast-like cells. Scale bars (A – D) = 100 µm; Scale bar (E) = 50 µm

TABLES

Table 1. Antibodies used for immunostaining.

Epitope	Host	Dilution	Supplier
ßIII tubulin	Rabbit	1:500	Biolegend; Poly18020
S100	Rabbit	1:500	Dako; Z0311
GFAP	Rabbit	1:500	Dako; Z0334
nNOS	Goat	1:1000	Abcam; ab1376
NF200	Rabbit	1:500	Sigma-Aldrich; N4142
Vimentin	Goat	1:50	Millipore; AB1620

PDGFR-α	Goat	1:200	R&D Systems ; AF1062
CD31	Rat	1:50	Abcam; ab56299
c-kit	Goat	1:1000	R&D Systems; AF1356
Calretinin	Rabbit	1:10000	Swant; CG1
Calbindin	Rabbit	1:2000	Swant; C858a138
Anti-rabbit Cy3	Donkey	1:400	Jackson Immunoresearch
Anti-goat Cy5	Donkey	1:400	Jackson Immunoresearch
Anti-rat Cy5	Donkey	1:400	Jackson Immunoresearch
Anti-rat Cy3	Donkey	1:400	Jackson Immunoresearch

Table 2: Comparison of properties of nine clearing protocols

Clearing protocol	Preservation		Clearing efficiency	IHC[a]	Handling	Time*	Safety
	GFP	Morphology					
Aqueous solution-based							
CUBIC	+	+	++	+++	+++	7d	+++
SeeDB2	+++	+++	+++	+++	+++	4d	+++
ScaleS	+	nd	+	nd	+++	4d	+++
Ce3D	+++	+++	+++	+++	+++	12 h	++
UbasM	++	nd	++	+++	+++	4d	+++
Hydrophobic solution-based							
3DISCO	+	+	+++	+++	+	4d	+
iDISCO+	-	+	+++	+++	+	5d	+
uDISCO	+	+	+++	+++	+	6d	+
Visikol	-	nd	+	nd	+	6d	+

+++= good; ++= medium; +=weak; -= not present; [a]= immunostaining; nd= not determined given the low clearing capacity; *= only incubation time of tissue permeabilization and/or tissue pretreatment and clearing procedures was considered without immunolabeling

Supplementary material

Supplementary figure. Similar images as shown in Figure 5, displaying the enteric nerve network (βIII-tubulin), the mononuclear phagocytes (CX3CR1), and the vascular

network (CD31) in UbasM-cleared (A, B and E) and SeeDB2-cleared intestinal segments (D, C). Note the inhomogeneous clearing capacity (asterisks) and the slightly lower immunostaining quality for the UbasM protocol (A,B). (C-E) Cross-sections of intestinal villi of CX3CR1 transgenic mice after SeeDB2 and UbasM clearing and immunostaining, respectively. Scale bar (B) = 100 µm, Scale bar (C, D, E)= 50 µm

Supplementary Video. 3D observation of the arrangement of the neurovascular network and the CX3CR1^{+} mononuclear phagocytes throughout the full thickness of the intestinal wall. Red: blood vessels stained by the endothelial marker CD31; green: GFP-labeled CX3CR1-positive mononuclear phagocytes; blue: the enteric nerve network visualized by means of ßIII-tubulin immunostaining; purple: nuclear (DAPI) staining.

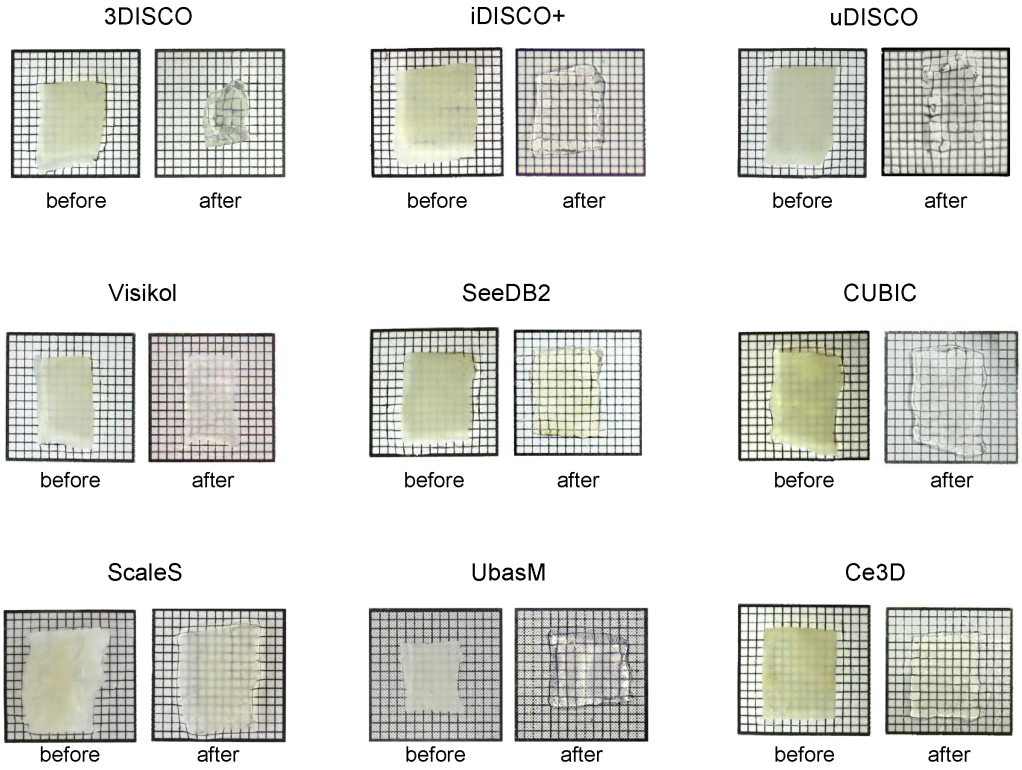
3DISCO
before
after
iDISCO+
before
after
uDISCO
before
after
Visikol
before
after
SeeDB2
before
after
CUBIC
before
after
ScaleS
before
after
UbasM
before
after
Ce3D
before
after

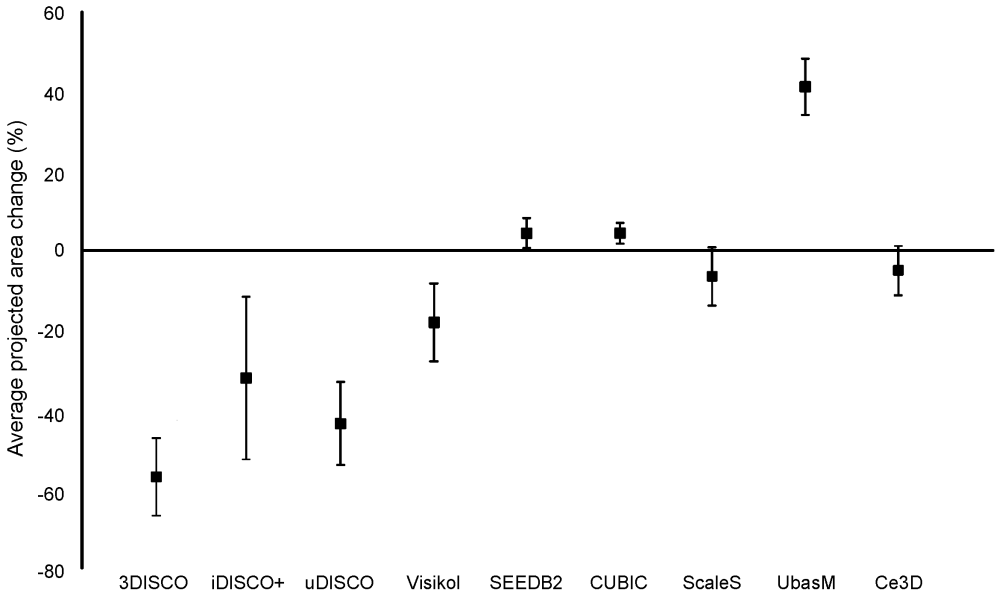
Average projected area change (%)
60
40
20
0
-20
-40
-60
-80
3DISCO
iDISCO+
uDISCO
Visikol
SEEDB2
CUBIC
ScaleS
UbasM
Ce3D

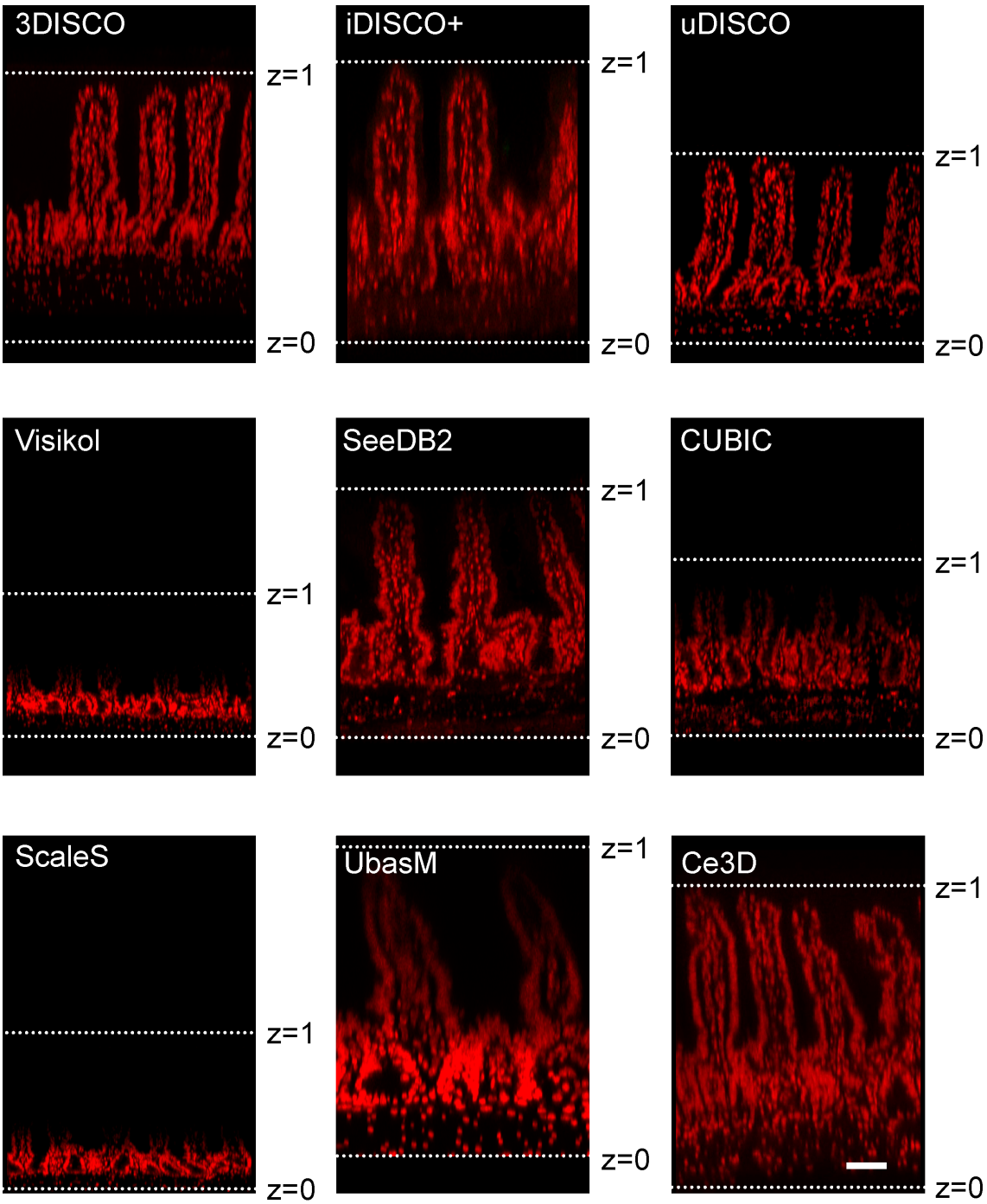
3DISCO
z=1
z=0
iDISCO+
z=1
z=0
uDISCO
z=1
z=0
Visikol
z=1
z=0
SeeDB2
z=1
z=0
CUBIC
z=1
z=0
ScaleS
z=1
z=0
UbasM
z=1
z=0
Ce3D
z=1
z=0

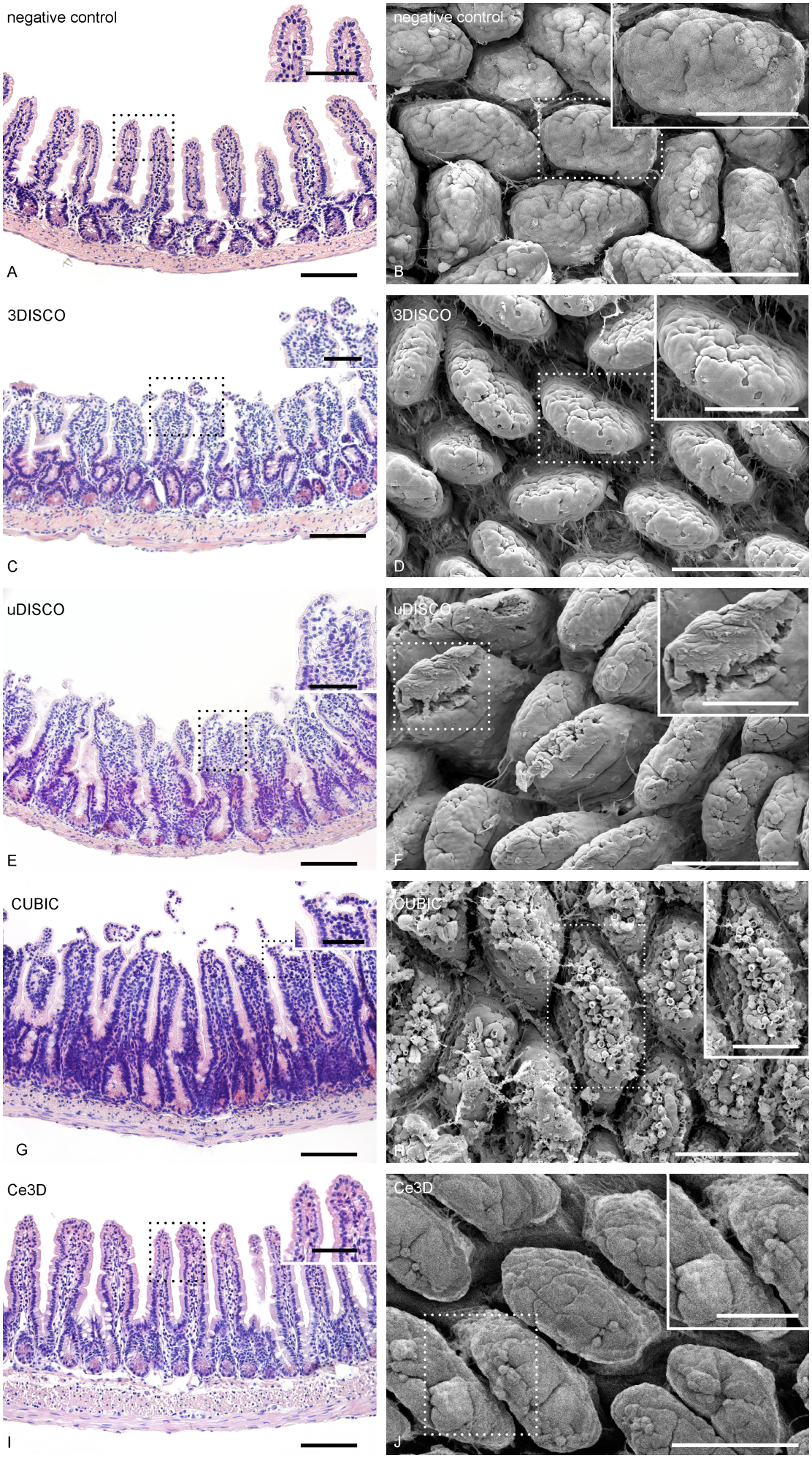
negative control
A
negative control
B
3DISCO
C
3DISCO
D
uDISCO
E
uDISCO
F
CUBIC
G
CUBIC
H
Ce3D
I
Ce3D
J

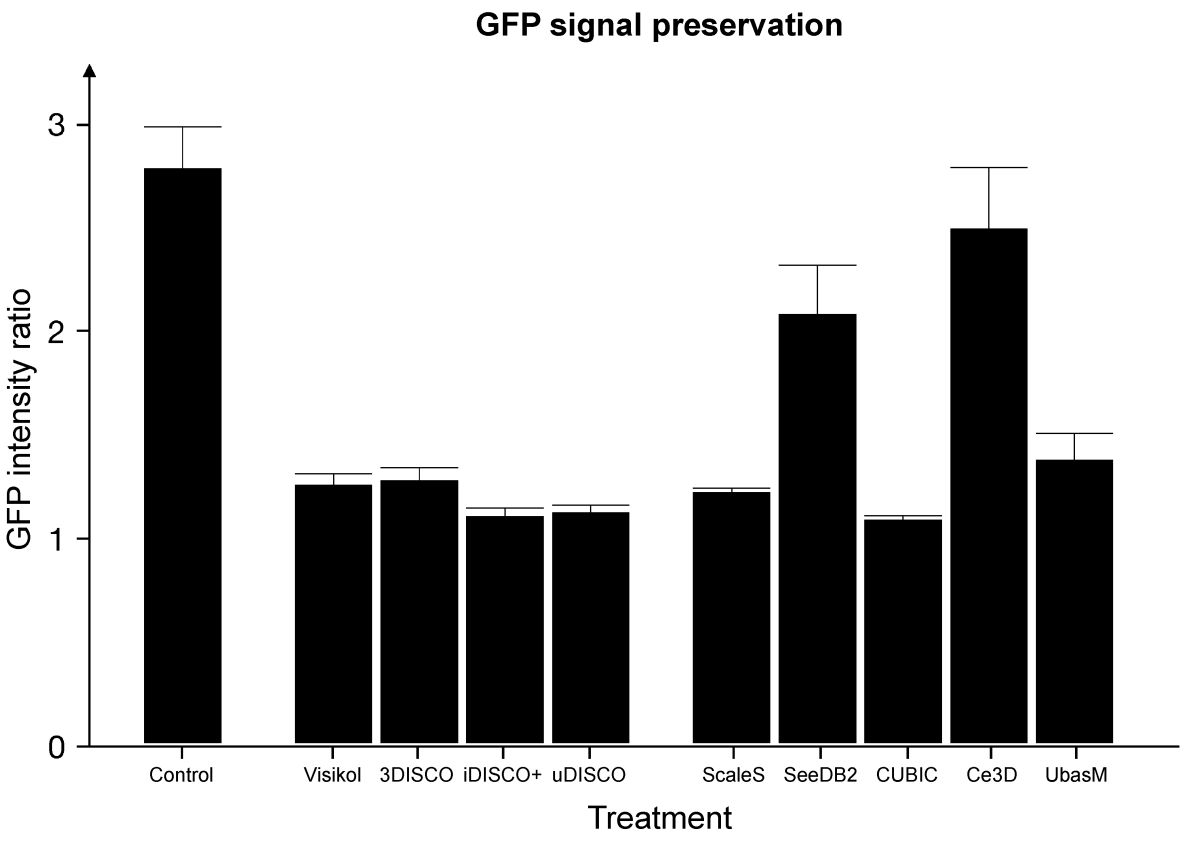
GFP signal preservation
GFP intensity ratio
0
1
2
3
Control
Visikol
3DISCO
iDISCO+
uDISCO
ScaleS
SeeDB2
CUBIC
Ce3D
UbasM
Treatment

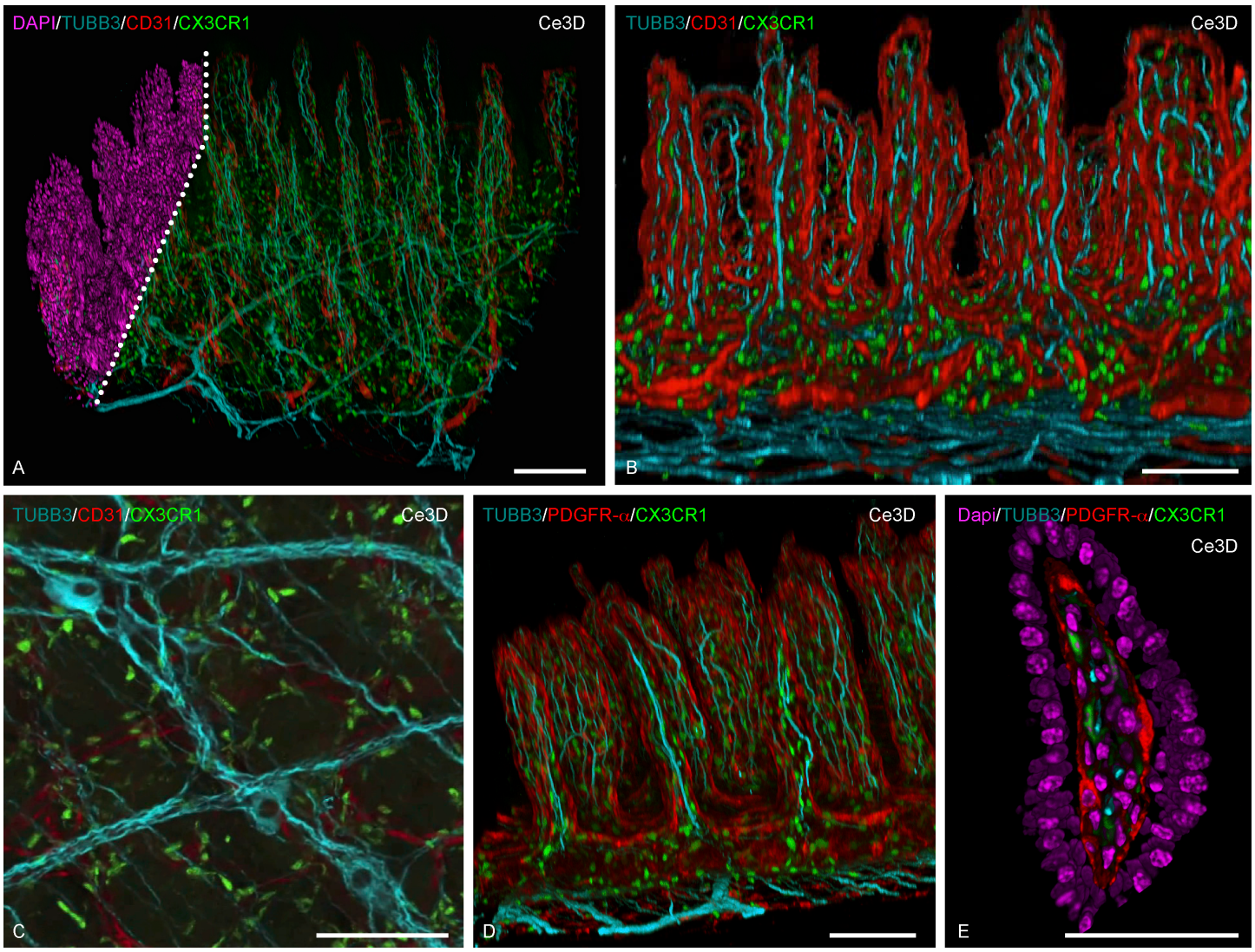
DAPI/TUBB3/CD31/CX3CR1
Ce3D
A
TUBB3/CD31/CX3CR1
Ce3D
B
TUBB3/CD31/CX3CR1
Ce3D
C
TUBB3/PDGFR-α/CX3CR1
Ce3D
D
Dapi/TUBB3/PDGFR-α/CX3CR1
Ce3D
E